

T1P3 - POSTER #10



T1P3 Poster #: 10



Exploring Mechanisms of Coke Formation and Migration for Increased Catalyst Stability

Joanna M. Rosenberger¹, Vamakshi Yadav¹, Brandon K. Bolton²,

Rajamani Gounder², Christina W. Li¹

¹Department of Chemistry, Purdue University

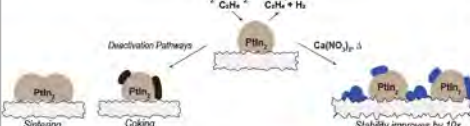
²Davidson School of Chemical Engineering, Purdue University



GOALS

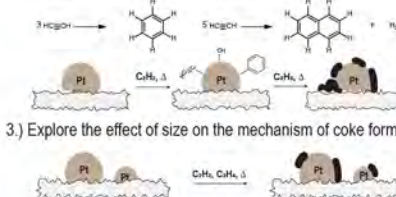
Bimetallic PtIn₂ catalysts exhibit >99% selectivity towards ethylene in ethane dehydrogenation at 600°C. However, these catalysts quickly deactivate due to coking. We are interested in **utilizing non-reducible metal-oxide shells to stabilize** PtIn₂/SiO₂ catalysts.

- 1.) Understand the effect of Ca doping on **reducing deactivation** of PtIn₂/SiO₂ catalysts



Relatively little is known about the **mechanisms of coke formation**. Understanding coke formation in different reaction conditions could assist in **new catalyst design** strategies.

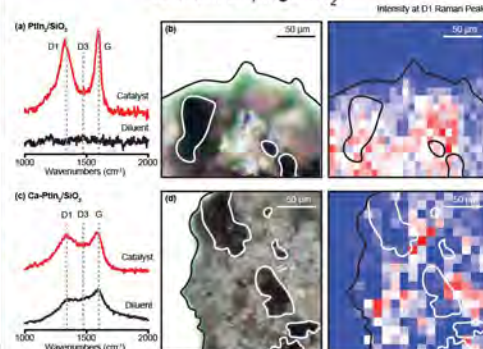
- 2.) Use acetylene oligomerization as a model reaction to probe initial differences in the mechanisms of coke formation



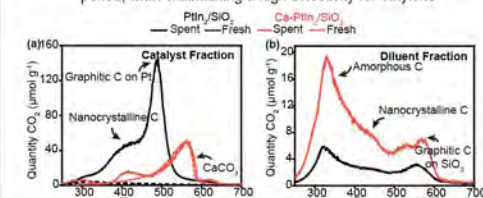
- 3.) Explore the effect of size on the mechanism of coke formation

MAIN FINDINGS

Calcium Doping PtIn₂

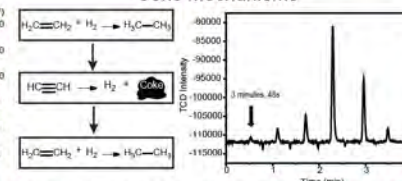


Ca doping into PtIn₂/SiO₂ **inhibits catalyst deactivation over 10x** over 24 hour period, while maintaining a high selectivity for ethylene

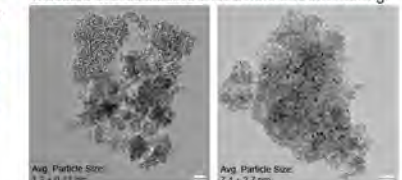


300-400°C: amorphous carbon deposits on silica
400-550°C: carbonaceous species on the metal and its vicinity
550-700°C: graphitized carbon, difficult to oxidize

Coke Mechanisms



Dehydrogenating acetylene results in the **production of hydrogen gas**. Pairing this method with **ethylene hydrogenation** can measure available active sites before and after coking.

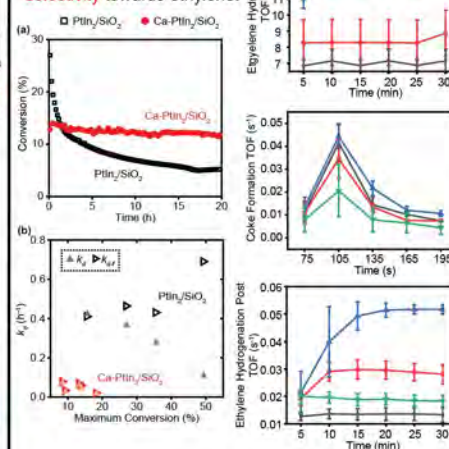


A variety of differently sized Pt nanoparticle catalysts can be synthesized via incipient wetness impregnation.

Sample	Weight Percent Pt	Calcination Temperature	Dispersion	Average Particle Size
iwi-250	0.5%	250°C	24.6%	3.3nm
iwi-300	2%	300°C	23.5%	1.9nm
iwi-600	2%	600°C	10.8%	5.2nm
iwi-Large	5%	600°C	7.7%	7.4nm

OUTCOMES

Ca-PtIn₂/SiO₂ reduces the inherent EDH deactivation rate of PtIn₂ nanoparticles by **8-fold** and maintains **>99% selectivity** towards ethylene.



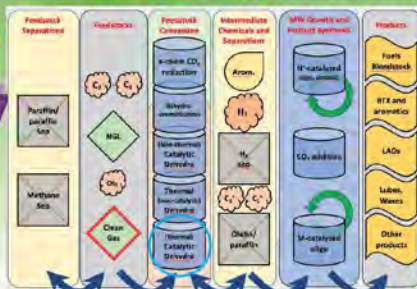
Catalyst size has little effect on coke formation rate or mechanism. Future systems of interest are PtM₂ alloys, different substrates, and Ca-doped catalysts.

IP & INNOVATION

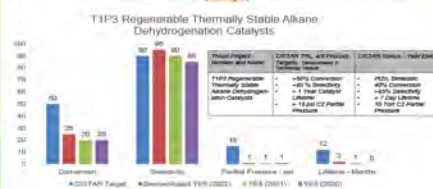
Understanding coke formation during early reaction stages is severely limited due to its rapid nature. Utilizing acetylene as a model dehydrogenation compound has not been studied before.



SYSTEM DESIGN & BENCHMARKS



Progress Toward CISTAR Target Catalyst



IMPACT & FUTURE

1. Ca doping strategy could easily be expanded to other catalysts of interest (PtSn)
2. Detailed characterization of coked catalyst samples will allow us to probe small molecules involved in coke formation
3. Understanding the differences in coke formation on different catalysts could assist in the design of more stable systems

T1P3 - POSTER #11



T1P3
Poster #: 11



Synthesis of Colloidal Platinum Alloys for Stable Alkane Dehydrogenation

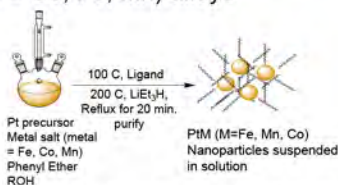
Nkem Azuka¹, Joanna Rosenberger¹, Christina Li¹

¹Department of Chemistry, Purdue University



GOALS

- Develop syntheses for colloidal PtM (M = Co, Fe, Mn) alloys



- Utilize colloidal alloys as catalysts instead of impregnated alloys for more stable ethane dehydrogenation



Shen, S., Anders, S., Thomson, T., Baglin, J. E. E., Torrey, M. F., Harrison, H. F., Murray, C. B., & Toste, G. D. (2013). Controlled Synthesis and Assembly of PtM Nanoparticles. *The Journal of Physical Chemistry B*, 117(23), 5419–5425. <https://doi.org/10.1021/jp121185>

Cheon, L. O., Yang, C., Lu, Z., Ren, Y., Zhang, Q., & Miller, J. T. (2019). Identification of a Pt₂Co Surface Intermetallic Alloy in Pt-Co Impregnated Dehydrogenation Catalysts. *ACS Catalysis*, 9(1), 5231–5244. <https://doi.org/10.1021/acscatal.8b02048>

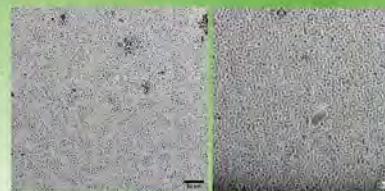
Esposito, N. J., Liberto, N. J., Miller, J. T., & Li, C. W. (2020). Colloidal Synthesis of Well-Defined Bimetallic Nanoparticles for Nonoxidative Alkane Dehydrogenation. *ACS Catalysis*, 10(17), 9813–9823. <https://doi.org/10.1021/acscatal.9c01104>

MAIN FINDINGS

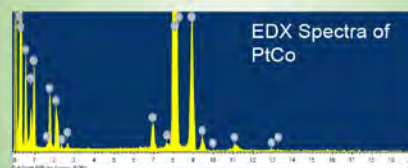
Platinum core, iron shell nanoparticles were synthesized. A low weight loading PtCo catalyst was synthesized.



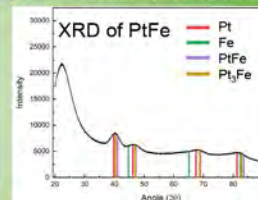
TEM Images
Left: PtCo
Right: PtFe



EDX reflects the entire particle. It is taken on a copper grid, hence the high signal among other contaminants, but the relative peak heights of Pt and Co corresponds well to the atomic percent.



Compound	Metal	EDX Average Atomic Percent	XRF Average Weight Percent
PtCo	Pt	0.39	0.04
	Co	0.62	0.07
PtFe	Pt	0.39	1.62
	Fe	0.50	0.54

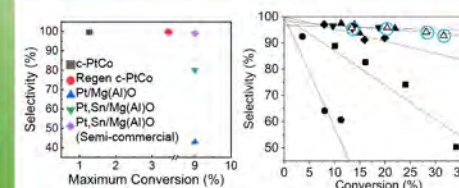


The XRD Spectra closely resembles Pt, despite the high Fe content. Since XRD does not reflect surface composition, the particle is likely a core-shell.



Fe shell, Pt core

OUTCOMES



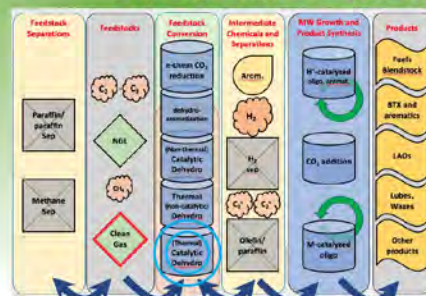
- Colloidal PtCo shows low conversion to ethylene that slightly improves after a regeneration.
- Likely due to remaining ligand migrating to the surface
- Selectivity remains high at 99%
- Better than more commercial Pt, Sn catalysts and impregnation PtCo (right, encircled in blue)

IP & INNOVATION

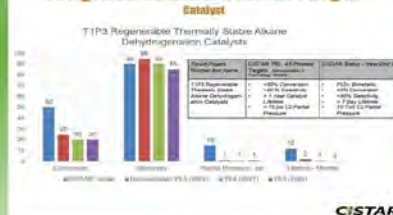
- Colloidal PtMn has not been synthesized. These methods will lead towards c-PtMn for ethane dehydrogenation



SYSTEM DESIGN & BENCHMARKS



Progress Toward CISTAR Target



IMPACT & FUTURE

- c-PtCo's high selectivity is promising for future colloidal catalysts
- Remove surface ligands for better conversions
- Synthesize homogeneous alloys of PtCo, PtFe and PtMn

T1P3 - POSTER #12



T1P3 Strategies to Mitigate Coke Formation and Buildup with Soft Oxidants *in situ* During PDH

Poster #: 12

Ryan Alcala¹, Shan Jiang², Stephen Porter¹, Brandon Burnside¹, Jeffrey T. Miller², Abhaya K. Datye¹

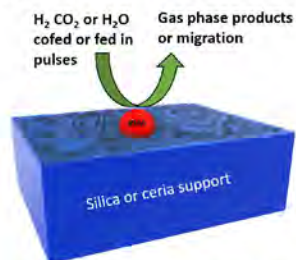
¹Department of Chemical and Biological Engineering, University of New Mexico

²Davidson School of Engineering, Purdue University



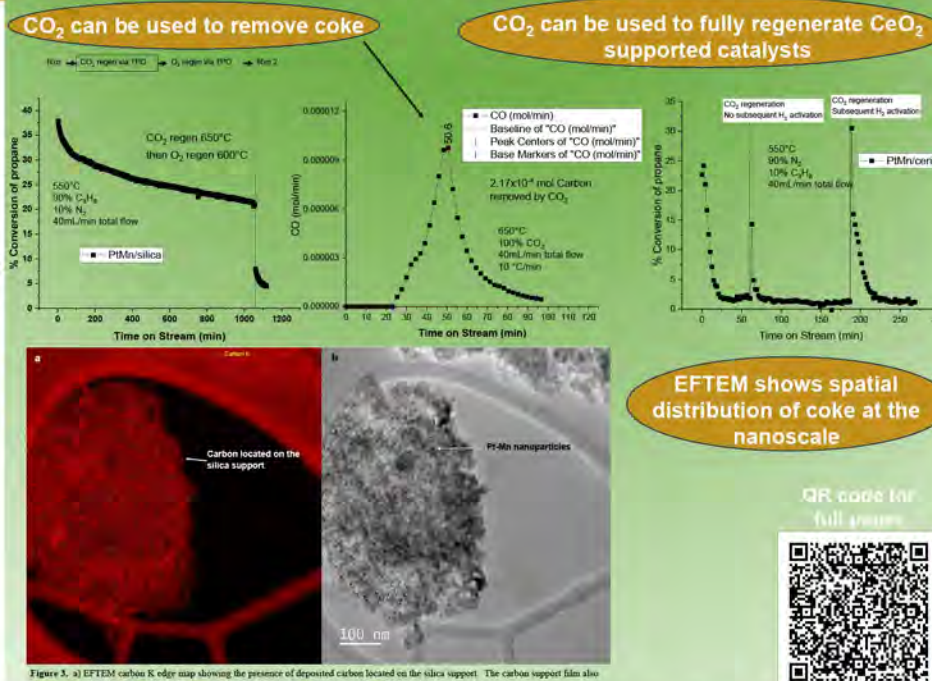
GOALS

- Investigate how soft oxidants can assist in regeneration and/or coke mitigation
- Develop procedures for effective regeneration of catalysts and *in situ* mitigation of coke
- Investigate the role of support on coke formation and its influence on catalyst deactivation



Can support interaction engineering provide novel regeneration strategies?

MAIN FINDINGS



OUTCOMES

- Mars-Van Krevelen like coke combustion may be responsible for ceria regenerability in CO₂
- Suggests *in situ* coke mitigation via reverse Boudouard reaction is possible
- Current studies are focused on CO₂ cofed experiments
 - $C_3H_8(g) \rightarrow C_3H_6(g) + H_2(g)$
 - $C_3H_6(g) \rightarrow 3C(s) + 3H_2(g)$
 - $CO_2(g) + C(s) \rightarrow 2CO(g)$

Hypotheses:

- Ceria-metal interface allows for facile combustion of adjacent coke via Mars Van Krevelen mechanism
 - allows catalyst to remain intact after oxidation
- CO₂ can remove coke from silica supported catalyst, but results in catalyst deactivation
 - Either coke is only removed from support or CO formed at temp accelerates sintering of the catalyst

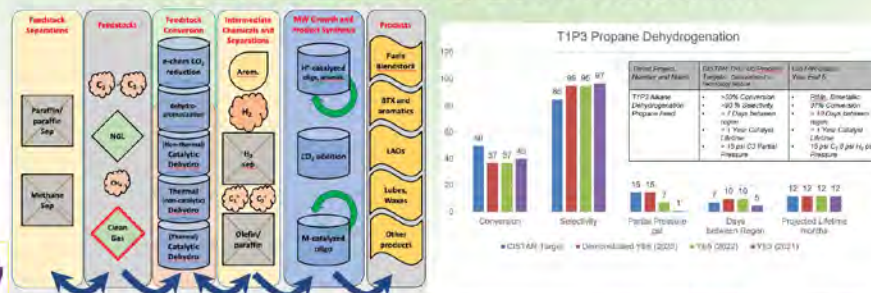


IP & INNOVATION

- Establishes a wide array of strategies to mitigate coke formation/accumulation
- Demonstrates support is effective at modifying the catalysis
- IP to be filed



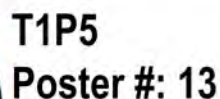
SYSTEM DESIGN & BENCHMARKS



IMPACT & FUTURE

- Allows for several strategies to be used for regeneration and/or coke mitigation making operation at the well-head possible
- H₂O gasification of coke *in situ* is next

T1P5 - POSTER #13



Denver Haycock, Russell Clarke, Jason Hicks, William Schneider
Department of Chemical and Biomolecular Engineering, University of Notre Dame



GOALS

The diagram illustrates the workflow of the ZDPlaskin software. It is divided into three main sections: INPUTS, KINETIC MODELING, and OUTPUTS.

INPUTS:

- Species, reactions, processes
- Rate constant information (Arrhenius or swarm)
- Reactor conditions ($T, P, N_{\text{in}}, E/N$)

KINETIC MODELING:

The central process is labeled "Kinetic modeling software ZDPlaskin". It is represented by a circle containing the differential equation:

$$\frac{d[N_i]}{dt} = \sum_{j=1}^{N_{\text{spec}}} Q_{ij}(t)$$

OUTPUTS:

- Temporally resolved:
 - Species densities with
 - Reaction rates
 - Reactor conditions ($T, P, N_{\text{in}}, E/N$)

Arrows indicate the flow of information from inputs to the modeling process and from the modeling process to the outputs.

The diagram illustrates a comparison between two industrial processes for producing ethylene (C_2H_4) from ethane (C_2H_6). The process starts with ethane (C_2H_6) on the left. Two curved arrows lead from it to two boxes. The top box, labeled 'Steam Cracking – current industry standard', lists: High temperatures, High pressure, and Non-selective. The bottom box, labeled 'Plasma Catalysis – TRL 1-2', lists: Ambient temperatures, Ambient pressure, High selectivity potential, and Electrically powered. A curved arrow leads from the top box to the right, where the products are listed: $C_2H_4 + H_2$. Another curved arrow leads from the bottom box to the same products, indicating a more efficient and selective process.

Steam Cracking – current industry standard

- High temperatures
- High pressure
- Non-selective

Plasma Catalysis – TRL 1-2

- Ambient temperatures
- Ambient pressure
- High selectivity potential
- Electrically powered

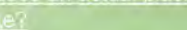
C_2H_6 → $C_2H_4 + H_2$

MAIN FINDINGS

The diagram shows three stages of plasma evolution:

- Initial ethane density:** A box labeled "initial ethane density" with $t < 0$ at the bottom. It contains numerous C_2H_6 molecules.
- plasma ignites, electrons introduced:** A box labeled "plasma ignites, electrons introduced" with $t = 0$ at the bottom. It shows C_2H_6 molecules and small blue dots representing electrons.
- speciation tracked over time:** A box labeled "speciation tracked over time" with $t > 0$ at the bottom. It shows a variety of chemical species including CH_4 , C_2H_4 , C_2H_2 , C_2H , C_2H_3 , C_2H_5 , C_2H_7 , C_2H_9 , C_2H_{11} , C_2H_{13} , C_2H_{15} , C_2H_{17} , C_2H_{19} , C_2H_{21} , C_2H_{23} , C_2H_{25} , C_2H_{27} , C_2H_{29} , C_2H_{31} , C_2H_{33} , C_2H_{35} , C_2H_{37} , C_2H_{39} , C_2H_{41} , C_2H_{43} , C_2H_{45} , C_2H_{47} , C_2H_{49} , C_2H_{51} , C_2H_{53} , C_2H_{55} , C_2H_{57} , C_2H_{59} , C_2H_{61} , C_2H_{63} , C_2H_{65} , C_2H_{67} , C_2H_{69} , C_2H_{71} , C_2H_{73} , C_2H_{75} , C_2H_{77} , C_2H_{79} , C_2H_{81} , C_2H_{83} , C_2H_{85} , C_2H_{87} , C_2H_{89} , C_2H_{91} , C_2H_{93} , C_2H_{95} , C_2H_{97} , C_2H_{99} , C_2H_{101} , C_2H_{103} , C_2H_{105} , C_2H_{107} , C_2H_{109} , C_2H_{111} , C_2H_{113} , C_2H_{115} , C_2H_{117} , C_2H_{119} , C_2H_{121} , C_2H_{123} , C_2H_{125} , C_2H_{127} , C_2H_{129} , C_2H_{131} , C_2H_{133} , C_2H_{135} , C_2H_{137} , C_2H_{139} , C_2H_{141} , C_2H_{143} , C_2H_{145} , C_2H_{147} , C_2H_{149} , C_2H_{151} , C_2H_{153} , C_2H_{155} , C_2H_{157} , C_2H_{159} , C_2H_{161} , C_2H_{163} , C_2H_{165} , C_2H_{167} , C_2H_{169} , C_2H_{171} , C_2H_{173} , C_2H_{175} , C_2H_{177} , C_2H_{179} , C_2H_{181} , C_2H_{183} , C_2H_{185} , C_2H_{187} , C_2H_{189} , C_2H_{191} , C_2H_{193} , C_2H_{195} , C_2H_{197} , C_2H_{199} , C_2H_{201} , C_2H_{203} , C_2H_{205} , C_2H_{207} , C_2H_{209} , C_2H_{211} , C_2H_{213} , C_2H_{215} , C_2H_{217} , C_2H_{219} , C_2H_{221} , C_2H_{223} , C_2H_{225} , C_2H_{227} , C_2H_{229} , C_2H_{231} , C_2H_{233} , C_2H_{235} , C_2H_{237} , C_2H_{239} , C_2H_{241} , C_2H_{243} , C_2H_{245} , C_2H_{247} , C_2H_{249} , C_2H_{251} , C_2H_{253} , C_2H_{255} , C_2H_{257} , C_2H_{259} , C_2H_{261} , C_2H_{263} , C_2H_{265} , C_2H_{267} , C_2H_{269} , C_2H_{271} , C_2H_{273} , C_2H_{275} , C_2H_{277} , C_2H_{279} , C_2H_{281} , C_2H_{283} , C_2H_{285} , C_2H_{287} , C_2H_{289} , C_2H_{291} , C_2H_{293} , C_2H_{295} , C_2H_{297} , C_2H_{299} , C_2H_{301} , C_2H_{303} , C_2H_{305} , C_2H_{307} , C_2H_{309} , C_2H_{311} , C_2H_{313} , C_2H_{315} , C_2H_{317} , C_2H_{319} , C_2H_{321} , C_2H_{323} , C_2H_{325} , C_2H_{327} , C_2H_{329} , C_2H_{331} , C_2H_{333} , C_2H_{335} , C_2H_{337} , C_2H_{339} , C_2H_{341} , C_2H_{343} , C_2H_{345} , C_2H_{347} , C_2H_{349} , C_2H_{351} , C_2H_{353} , C_2H_{355} , C_2H_{357} , C_2H_{359} , C_2H_{361} , C_2H_{363} , C_2H_{365} , C_2H_{367} , C_2H_{369} , C_2H_{371} , C_2H_{373} , C_2H_{375} , C_2H_{377} , C_2H_{379} , C_2H_{381} , C_2H_{383} , C_2H_{385} , C_2H_{387} , C_2H_{389} , C_2H_{391} , C_2H_{393} , C_2H_{395} , C_2H_{397} , C_2H_{399} , C_2H_{401} , C_2H_{403} , C_2H_{405} , C_2H_{407} , C_2H_{409} , C_2H_{411} , C_2H_{413} , C_2H_{415} , C_2H_{417} , C_2H_{419} , C_2H_{421} , C_2H_{423} , C_2H_{425} , C_2H_{427} , C_2H_{429} , C_2H_{431} , C_2H_{433} , C_2H_{435} , C_2H_{437} , C_2H_{439} , C_2H_{441} , C_2H_{443} , C_2H_{445} , C_2H_{447} , C_2H_{449} , C_2H_{451} , C_2H_{453} , C_2H_{455} , C_2H_{457} , C_2H_{459} , C_2H_{461} , C_2H_{463} , C_2H_{465} , C_2H_{467} , C_2H_{469} , C_2H_{471} , C_2H_{473} , C_2H_{475} , C_2H_{477} , C_2H_{479} , C_2H_{481} , C_2H_{483} , C_2H_{485} , C_2H_{487} , C_2H_{489} , C_2H_{491} , C_2H_{493} , C_2H_{495} , C_2H_{497} , C_2H_{499} , C_2H_{501} , C_2H_{503} , C_2H_{505} , C_2H_{507} , C_2H_{509} , C_2H_{511} , C_2H_{513} , C_2H_{515} , C_2H_{517} , C_2H_{519} , C_2H_{521} , C_2H_{523} , C_2H_{525} , C_2H_{527} , C_2H_{529} , C_2H_{531} , C_2H_{533} , C_2H_{535} , C_2H_{537} , C_2H_{539} , C_2H_{541} , C_2H_{543} , C_2H_{545} , C_2H_{547} , C_2H_{549} , C_2H_{551} , C_2H_{553} , C_2H_{555} , C_2H_{557} , C_2H_{559} , C_2H_{561} , C_2H_{563} , C_2H_{565} , C_2H_{567} , C_2H_{569} , C_2H_{571} , C_2H_{573} , C_2H_{575} , C_2H_{577} , C_2H_{579} , C_2H_{581} , C_2H_{583} , C_2H_{585} , C_2H_{587} , C_2H_{589} , C_2H_{591} , C_2H_{593} , C_2H_{595} , C_2H_{597} , C_2H_{599} , C_2H_{601} , $C_$

What does an actual plasma reactor look like?

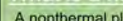


These are photos of plasma and plasma catalytic reactors in use at the University of Notre Dame for CISTAR projects.

Various parameters—including reactor temperature, flow rates, solid packing, and electric power—can be manipulated and tested.

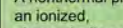
What is a nonthermal plasma, why do we use it?

A nonthermal plasma is an ionized, electronically-conductive gas



Enables electrified reactor processes

- Relatively high density of free, hot electrons, ions, and radicals
- Electrically driven energy input
- Bulk gas temperature remains low



Nonthermal chemistry allows for less extreme process conditions

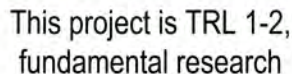
Industrially used for ozone production.

OUTCOMES

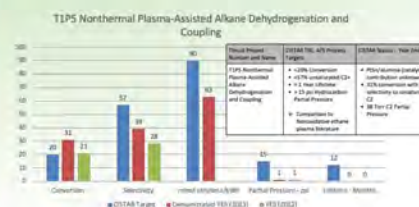
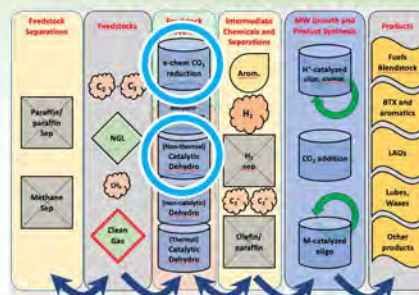
Scan for an example from the literature showing kinetic modeling results for an ethane + CO₂ nonthermal plasma



IP & INNOVATION



SYSTEM DESIGN & BENCHMARKS



IMPACT & FUTURE

Test sensitivity to:

- Plasma conditions (E/N , N_e)
- Gas compositions (T , diluent)
- Time scales
- Initial conditions
- Reactor configuration

T1P5 - POSTER #14



**T1P5
Poster #: 14**



Low-Temperature Olefin/Liquid Production and Coke Suppression in Light Alkane Plasmas

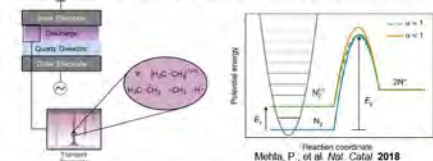
Russell J. Clarke¹ and Jason C. Hicks^{1*}

¹Department of Chemical and Biomolecular Engineering, University of Notre Dame

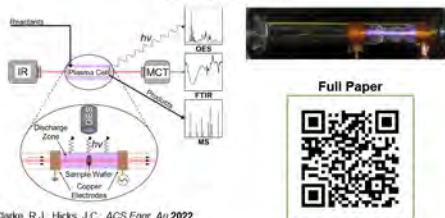


GOALS

Plasma Forms Reactive Species and Lowers Dissociation Barrier

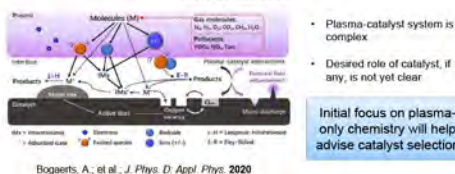


Y5 Goal: Develop a Spectroscopic Tool to Observe Plasma-Surface Interactions



Clarke, R.J., Hicks, J.C., ACS Engr. Au 2022

Y6-7 Goal: Determine Drivers of Selectivity and Stability to Inform Catalyst Selection

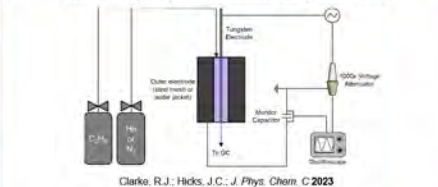


Bogaerts, A., et al., J. Phys. D: Appl. Phys. 2020

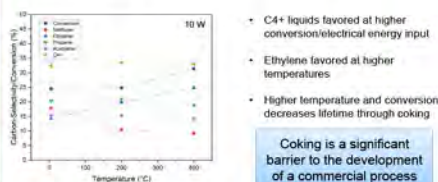
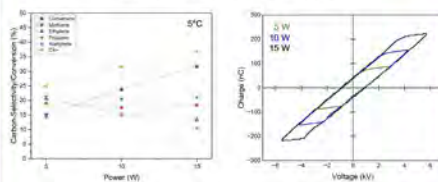
MAIN FINDINGS

Insight into coking process in alkane plasmas led to control over carbon formation and enhanced stability

Ethane Dehydrogenation and Coupling Below 298 K



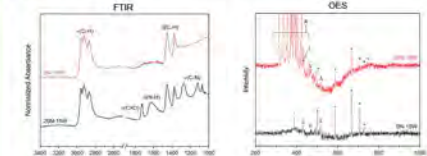
Clarke, R.J., Hicks, J.C., J. Phys. Chem. C 2023



- C4+ liquids favored at higher conversion/electrical energy input
- Ethylene favored at higher temperatures
- Higher temperature and conversion decreases lifetime through coking

Coking is a significant barrier to the development of a commercial process

Synthesis Patterns of Diamond-Like Carbon Microrods (Coke)



Clarke, R.J., Hicks, J.C., J. Phys. Chem. C 2023

- Microrods have little aromaticity and high sp³ bonding (diamond-like)
- Growth spacing from electrode to dielectric dictated by microdischarge pattern

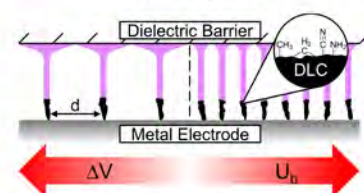
Carbon formation can be controlled through adjustments to plasma properties

Full Paper



OUTCOMES

Carbon Growth Spacing Can Be Controlled by Tuning Plasma Properties



Clarke, R.J., Hicks, J.C., J. Phys. Chem. C 2023

Carbon Growth Can Be Slowed or Inhibited Through Minor Changes to the Plasma/Reaction Conditions



Normal Conditions

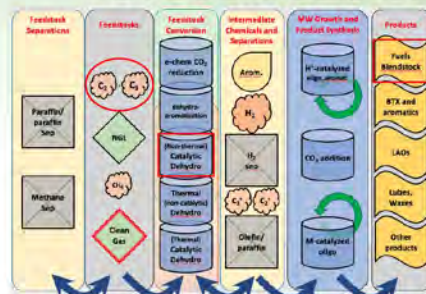
Coke Suppressing Conditions

IP & INNOVATION

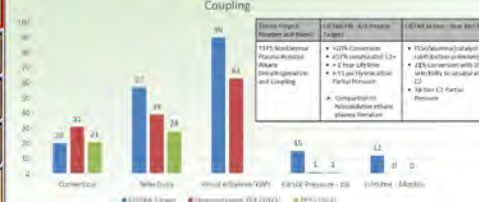


- Developed technique for suppressing coke in alkane plasmas
- Understand catalyst role in plasma-assisted alkane dehydrogenation

SYSTEM DESIGN & BENCHMARKS

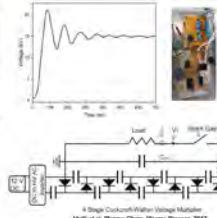


T1P5 Nonthermal Plasma-Assisted Alkane Dehydrogenation and Coupling

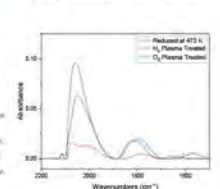


IMPACT & FUTURE

Nanosecond Pulsed Power for More Efficient Power Delivery



Catalyst Characterization Post-Reaction and/or Post-Regeneration with Plasma



T2P1 - POSTER #15



T2P1 Poster #: 15



Isolating Kinetic Effects of Void Environment in MFI Zeolites on Transport-Limited Propene Oligomerization

Lauren Kilburn¹, Diamarys Salomé Rivera¹, David Hibbits¹, Rajamani Gounder

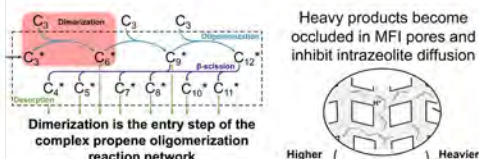
¹Davidson School of Chemical Engineering, Purdue University

²Department of Chemical Engineering, University of Florida



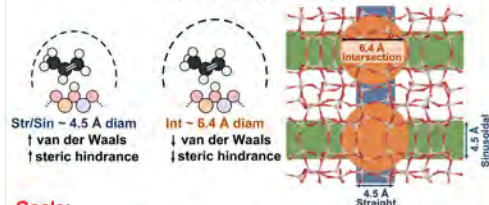
GOALS

- H-MFI zeolite catalyzed propene oligomerization reaction



Challenge: Propene oligomerization kinetics in MFI zeolites are coupled with transport limitation effects

Al location is a tunable property in MFI zeolites that may influence reaction kinetics



Goals:

- Combine a computational and experimental approach to study the independent effect of Al location in propene oligomerization rates, selectivity and deactivation behavior.
- Identify promising samples for the oligomerization Testbed

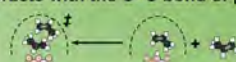
MAIN FINDINGS

Al location in MFI can influence dimerization kinetics during propene oligomerization

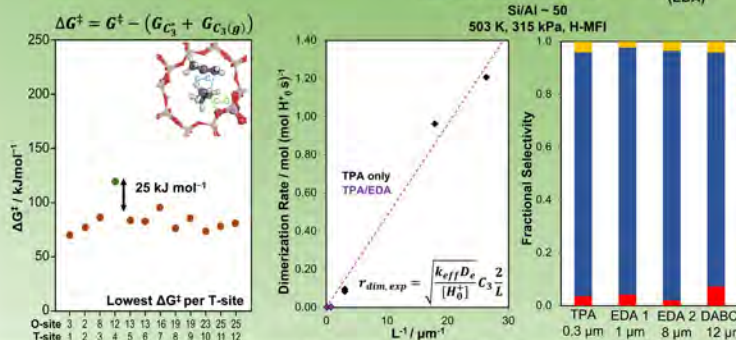
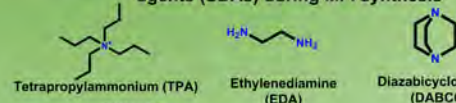
Al atoms site at 12 crystallographically unique tetrahedral sites (T-sites) in MFI

T-site:	1	2	3	4	5	6	7	8	9	10	11	12
Int:	x	x	x	x	x	x	x	x	x	x	x	x
Sin:	x	x	x	x	x	x	x	x	x	x	x	x
Str:	x	x	x	x	x	x	x	x	x	x	x	x

Propene dimerization transition state involves the formation of a carbocation that interacts with the C=C bond of propene



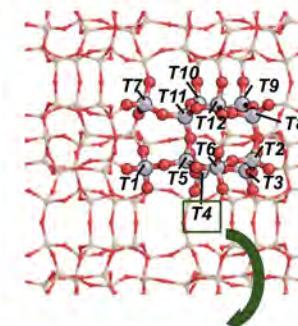
Al location can be varied using structure directing agents (SDAs) during MFI synthesis



QR Code for Full Poster



OUTCOMES



T4—the only T-site without access to the intersection—has the highest ΔG[‡] of the 12 T-sites by 25 kJ mol⁻¹

- DFT suggest dimerization rates will decrease if an SDA preferentially sites Al at T4
- Void environment weakly influences the stability of C₃ and C₆ adsorbates across T-sites (ΔG_{Ads} range of ~20 kJ mol⁻¹) when only the most favorable species are considered
- Preliminary selectivity data shows similar product distribution for samples synthesized with different SDAs

IP & INNOVATION

- Identify and optimize catalyst properties that result in high yields and selectivity to higher molecular weight olefins under testbed conditions

- Provisional patent application for:

Stable Product Oligomer Selectivity From Olefin Oligomerization on ZSM5-5 Zeolites and Zeotypes.
Rajamani Gounder, Elizabeth Bickel, Songhyun Lee, Evan Sowinski U. S. Patent Application No.63/445,206 (2023)

SYSTEM DESIGN & BENCHMARKS



IMPACT & FUTURE

- Provide mechanistic explanations for differences in dimerization rates and selectivity during propene oligomerization as catalyst properties (e.g., Al location in MFI) are varied.
- This study provides fundamental insights that can guide catalyst design for upgrading hydrocarbons.
- Future work will involve further experimental measurements on MFI samples synthesized with different SDAs. Observed trends will be compared to DFT-predicted results to assess the influence of transport effects

T2P1 - POSTER #17

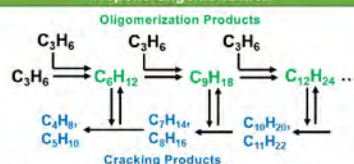


T2P1
Poster #: 17



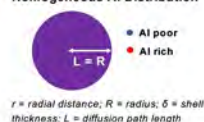
GOALS

Propene Oligomerization



- Crystallite-scale Al distribution (external sites, zoning) also affects rates, selectivity, and deactivation during olefin oligomerization.

Homogeneous Al Distribution



Thiele Modulus = $\frac{\text{Reaction Rate}}{\text{Diffusion Rate}}$

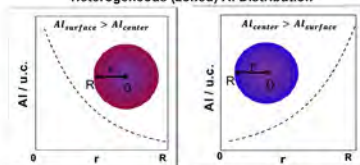
Catalyst Active site properties

$$= \frac{[H]^2 L^2}{De} \times k$$

Diffusion parameter = $[H]^2 L^2$

Challenge: No well-defined boundary of spatial Al distribution.

Heterogeneous (zoned) Al Distribution



Objective: Tune the diffusion path length by biasing the spatial Al distribution using core@shell synthesis methods to influence olefin oligomerization rates and product selectivity.

IP & INNOVATION

- Develop core@shell zeolite synthesis methods to bias Al spatial distribution toward or away from external crystallite surfaces, to alter the effects of coupled reaction-diffusion phenomena and pathways that cause deactivation



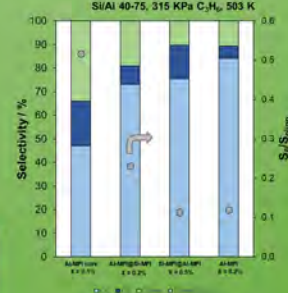
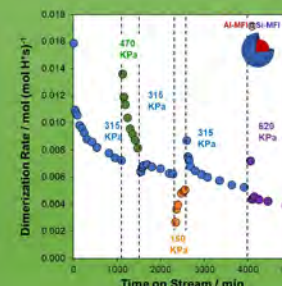
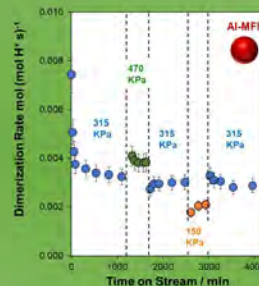
Heterogeneous distribution of acid-site regulates diffusional constraints governing propene oligomerization deactivation

Ricem Diaz Arroyo¹, Elizabeth Bickel¹, Rajamani Gounder¹

¹Department of Chemical Engineering, Purdue University

MAIN FINDINGS

Crystallite-scale Al distribution influences the selectivity and deactivation profile during propene oligomerization.



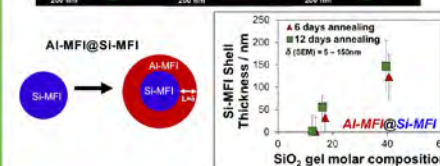
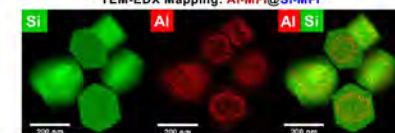
QR Code for Full Paper



OUTCOMES

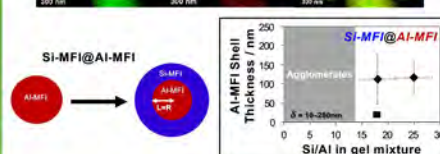
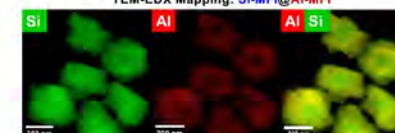
Al-MFI@Si-MFI Synthesis

TEM-EDX Mapping: Al-MFI@Si-MFI

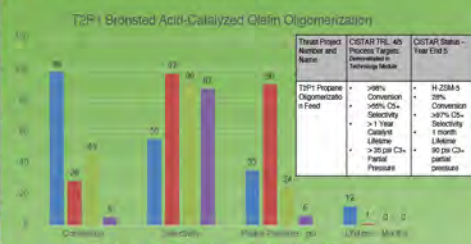
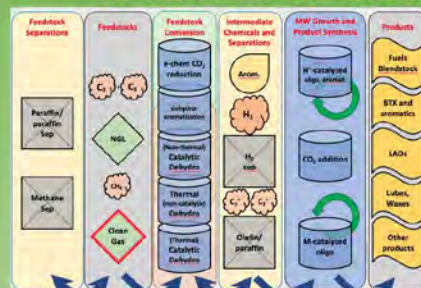


Si-MFI@Al-MFI Synthesis

TEM-EDX Mapping: Si-MFI@Al-MFI



SYSTEM DESIGN & BENCHMARKS



IMPACT & FUTURE

- Identify effects of solid material properties such as Al spatial zoning, crystallite size and diffusion parameter on olefin oligomerization rate, product selectivity and deactivation behavior.
- Future: Assess the influence of crystallite-scale Al distribution on diffusion limitations through transient changes in observed rates upon step changes of reactant pressure.

T2P4 - POSTER #18



T2P4
Poster #: 18



Effects of Ethene Pressure on the Deactivation of Nickel Active Sites Exchanged on Porous Aluminosilicate Materials During Ethene Oligomerization

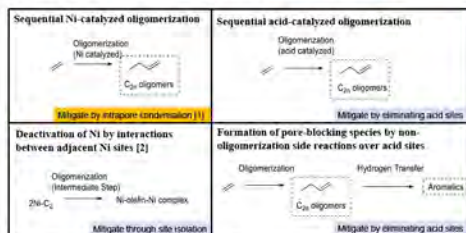
Richard Caulkins¹, Christian Borrero Villalob¹, Fabio Ribeiro¹, Rajamani Gounder¹

¹ Davidson School of Chemical Engineering, Purdue University

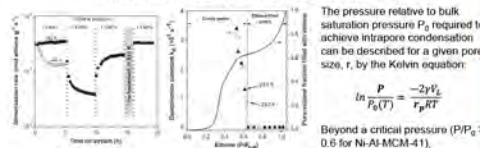
CISTAR
NSF Engineering Research Center
Center for Innovative and Strategic Transformation of Alkane Resources

GOALS

- Ni-exchanged zeolites catalyze alkene oligomerization at low temperatures but rapidly deactivate.
- This work is motivated by the need to develop catalysts and/or reaction conditions which can achieve CISTAR stability target
- Several mechanisms explain this deactivation; some pathways can be eliminated via *synthetic approaches*, while other deactivation pathways are better handled through choosing appropriate *reaction conditions*.



Intrapore condensation (i.e., when confinement effects within mesoporous and microporous materials cause a fluid to form a liquid-like phase within a pore at pressures below bulk saturation pressures) significantly reduces deactivation in Ni-AI-MCM-41 during ethene oligomerization. [1]



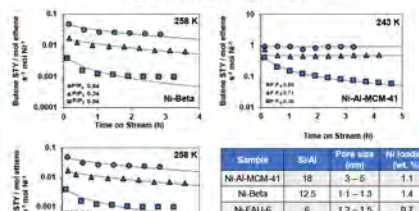
[1] Agrawal, Telenia and Iglesia, J. Catal. 352 (2017) 505-514
[2] A. Menar et al., J. Catal. 296 (2012) 156-164

Deactivation via formation of heavy oligomers over Ni sites can be mitigated in Ni-AI-MCM-41 by operating under capillary condensation conditions; can this principle be generalized to CISTAR Ni-exchanged zeolites?

MAIN FINDINGS

Deactivation is mitigated under capillary condensation conditions in (mesoporous) Ni-AI-MCM-41 but not in Ni-exchanged (microporous) zeolites at conditions that should lead to capillary condensation

A series of Ni-exchanged aluminosilicates (zeolites and mesoporous AI-MCM-41) with varying pore diameters were prepared: Ni-Beta < Ni-FAU-6 < Ni-AI-MCM-41



¹ Ni was co-fed (1% of total feed) during Ni-FAU experiments. Dashed lines represent fits of deactivation models.

Sample	Si/Al	Pore size (nm)	Ni loading (wt. %)
Ni-AI-MCM-41	19	3-5	1.1
Ni-Beta	12.5	1.1-1.3	1.4
Ni-FAU-6	6	1.2-1.5	0.7

Deactivation orders and constants can be calculated for each catalyst and pressure [3].
 $r = \frac{P}{P_s}$
 $(1 + (n-1)k_d r^{n-1})e^{-1}$

Solution of products mediated by an intrapore condensed phase is demonstrated by an abrupt drop in deactivation constant in Ni-AI-MCM-41, but this drop is not observed in Ni-exchanged zeolites.

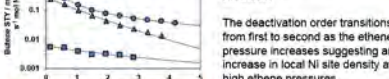
Ni site density needs to be evaluated to confirm that capillary condensation has no effect on deactivation in Ni-exchanged microporous zeolites.

[3] J. Butt, Activation, Deactivation, and Poisoning of Catalysts, Elsevier, San Diego, 2012

Decreasing site density reveals a transition in deactivation order in Ni-FAU-40 (Si/Al = 40) as a function of ethene pressure

Sample	Pore diameter (nm)	Ni loading (wt. %)	Ni site density (sites/nm ²)	Avg. Ni-Ni distance (nm)
Ni-FAU-6	1.2-1.5	0.7	0.33	1.3
Ni-FAU-40	1.4-1.7	0.3	0.12	2.6

Ni sites in Ni-FAU-40 are more isolated than Ni sites in Ni-FAU-6, as shown by estimated Ni-Ni site distances.



The deactivation order transitions from first to second as the ethene pressure increases suggesting an increase in local Ni site density at high ethene pressures.

Ni-FAU-40 deactivates regardless of the conditions studied indicating capillary condensation conditions do not influence the deactivation behavior.

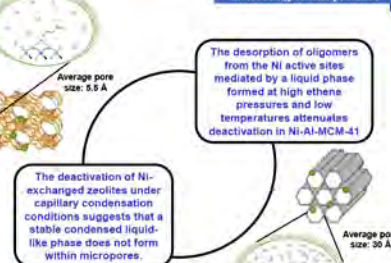
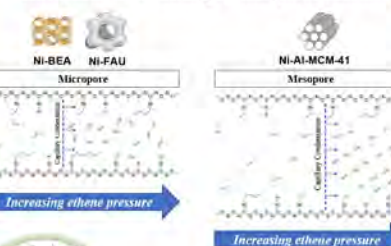
The transition from a first-order to a second-order deactivation behavior with increasing ethene pressure could be a combined effect of increased generation of active Ni(II)-alkyl sites [4] influenced by initial density and by the mobilization of Ni sites under high ethene pressures [5].

[4] Savens et al., ACS Eng. Au (2021)

[5] Brogaard et al., ACS Catal. 9 (2019) 5645-5650

OUTCOMES

Capillary condensation does not attenuate deactivation in Ni-exchanged microporous zeolites



The results from this work motivate efforts to develop synthetic methods and establish reaction conditions at which Ni-exchanged catalysts are stable and industrially viable.

IP & INNOVATION

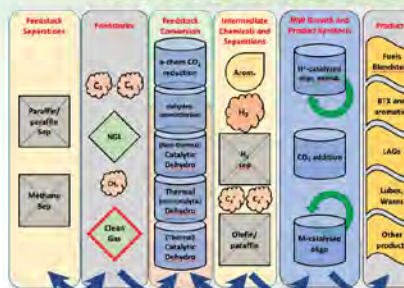
- Current efforts seek to develop materials that show behaviors (during alkene oligomerization) that are different to those already reported in literature and that are industrially applicable.
- Intellectual property documentation will be filed upon the design of a material relevant to CISTAR's main goals.



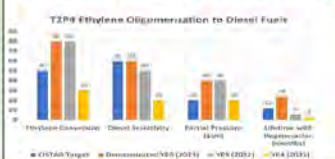
QR Code for Full Paper



SYSTEM DESIGN & BENCHMARKS



Progress Toward CISTAR Target



T2P4 Ethylene Oligomerization to Diesel Fuels
CISTAR Target: 44% Diesel, 56% Gasoline
Current Performance: 37% Diesel, 63% Gasoline
CISTAR Target: 44% Diesel, 56% Gasoline
Current Performance: 37% Diesel, 63% Gasoline

IMPACT & FUTURE

Ni-AI-MCM-41 exhibits stable behavior during ethene oligomerization due to capillary condensation.

Capillary condensation does not attenuate deactivation in Ni-exchanged microporous zeolites, suggesting that only mesoporous materials have pores sufficiently large to support a solvating phase of ethene.

High ethene pressures result in a shift in deactivation mechanism in microporous Ni zeolites from a first-order mechanism, where heavy molecular weight species form over single Ni sites, to a second-order mechanism, where a bridging alkyl species forms between two proximal Ni sites.

These results generate new research questions regarding mesoporous materials. Can other mesoporous Ni catalysts be stabilized under condensation conditions? Could the capillary condensation regime be altered in Ni-AI-MCM-41 by functionalizing these materials?

Future work will focus on mesoporous catalysts such as Ni-POM materials dispersed within mesoporous SBA-15 and functionalized Ni-AI-MCM-41 developed in collaboration with colleagues at Notre Dame and Northwestern University.

T2P4 - POSTER #19



T2P4 Poster #: 19



Tuning the Structure of Nickel-Substituted Polyoxometalates for Ethene Oligomerization

Alba Scotto d'Apollonia¹, Yoonrae Cho¹, Allen Oliver², Jason C. Hicks^{1*}

¹Department of Chemical and Biomolecular Engineering, University of Notre Dame

²Department of Chemistry and Biochemistry Engineering, University of Notre Dame

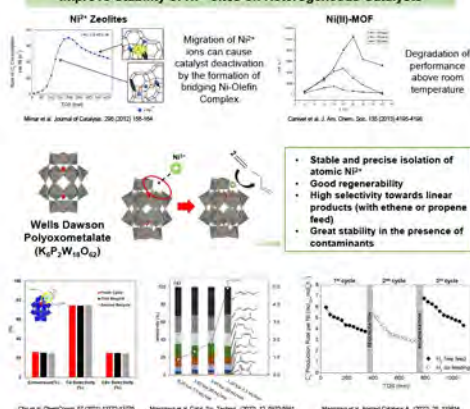


NSF Engineering Research Center

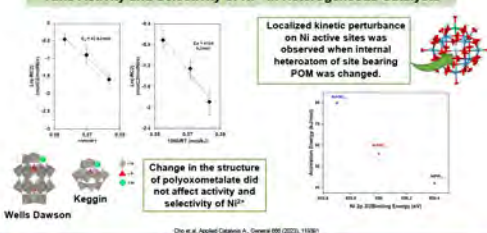
Center for Innovative and Strategic Transformation of Alkane Resources

GOALS

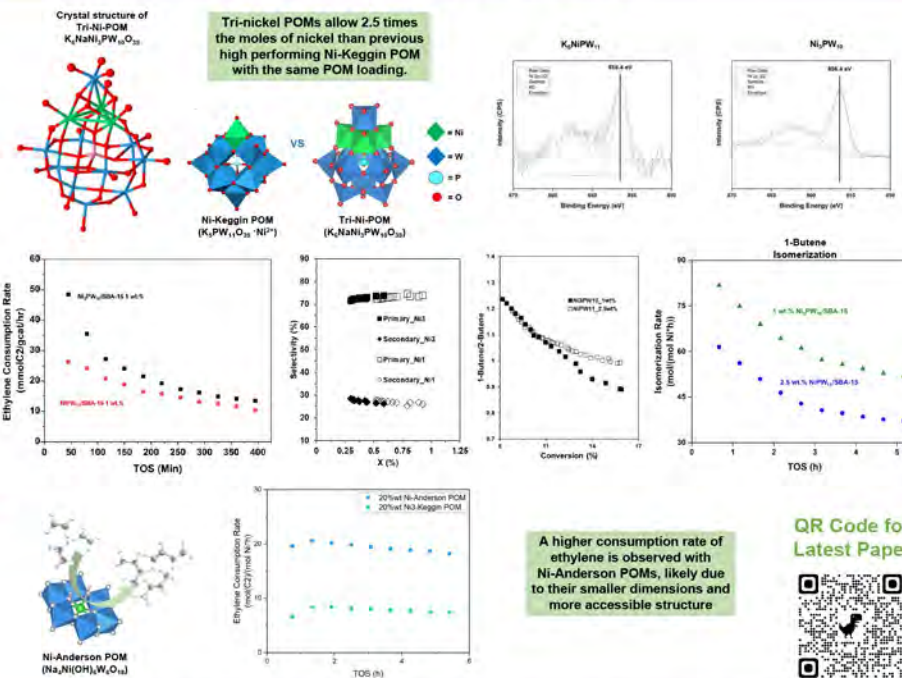
Improve Stability of Ni²⁺ sites on Heterogeneous Catalysts



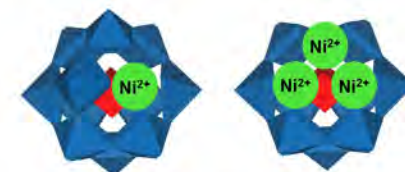
Tune Activity and Selectivity of Ni²⁺ in Heterogeneous Catalysts



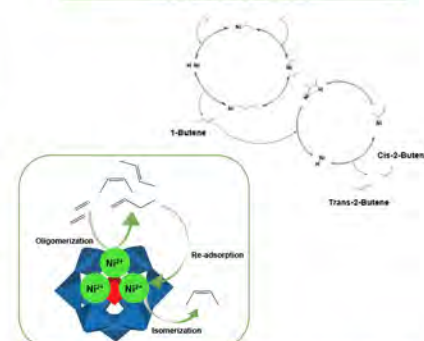
MAIN FINDINGS



OUTCOMES



By tuning the structure of the polyoxometalate platforms the loading limitations of nickel in the catalyst can be mitigated.

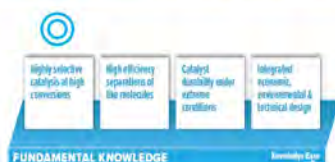


The high proximity of Ni²⁺ sites favors the isomerization of 1-butene to 2-butene.

QR Code for Latest Paper

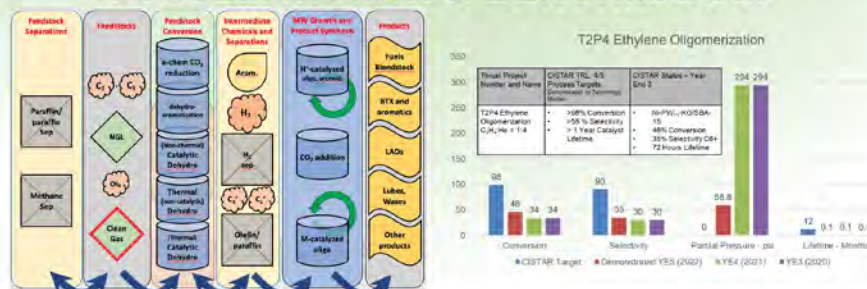


IP & INNOVATION



- Design catalysts highly selective towards linear products.
- Improve conversion per mass of catalyst.
- Understand underlying properties of polyoxometalates that can be applied to promote olefin oligomerization.

SYSTEM DESIGN & BENCHMARKS



IMPACT & FUTURE

IMPACT

The structural modifications implemented on polyoxometalate platforms allow for a higher loading of Ni²⁺ sites in the catalyst, which will contribute towards the CISTAR target conversion.

FUTURE

Further exploration of the structural modifications on polyoxometalates will be conducted to permit the tunability of the catalyst for target applications. This will also improve the understanding of these materials, aiding future catalyst design.

T2P4 - POSTER #20



T2P4
Poster #: 20



Computational Exploration of the Catalytic Activity of Single Site Polyoxometalates for Oligomerization Reactions

Michael Appoh¹, William Schneider^{1,2}

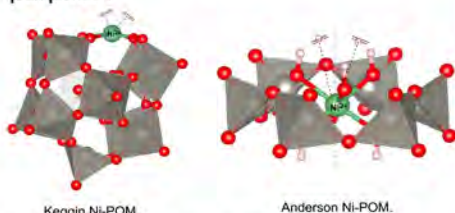
¹Department of Chemistry and Biochemistry, University of Notre Dame

²Department of Chemical Engineering, University of Notre Dame



GOALS

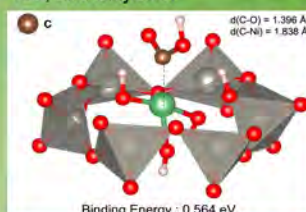
- 'Heterogeneous' single site catalysts shows promising route to controllable to practical ethylene oligomerization reaction.
- POM provides a tunable and heterogenizable platform for such purpose.



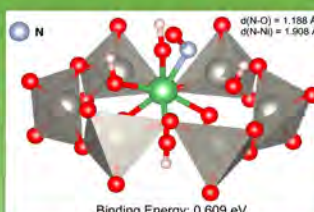
- Explore the structure of the two polyoxometalate and their accessibility, particularly, their affinity with target adsorbate using Density Functional Theory (DFT).

MAIN FINDINGS

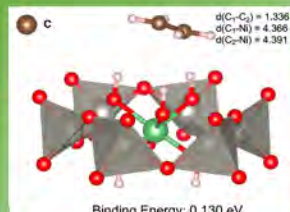
- To test our model and provide insight into the performance of these single site catalyst, we explored two polyoxometalate classes, Anderson and Keggin, focusing on their interactions with target adsorbates: CO, NO, and ethylene.



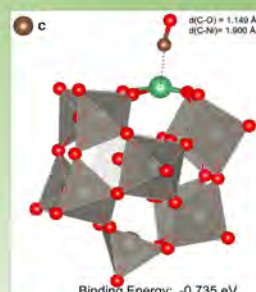
CO Anderson Ni-POM.



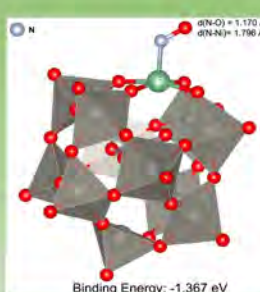
NO on Anderson Ni-POM.



Ethylene on Anderson Ni-POM.



CO on Keggin Ni-POM.



NO on Keggin Ni-POM.



Ethylene on Keggin Ni-POM.

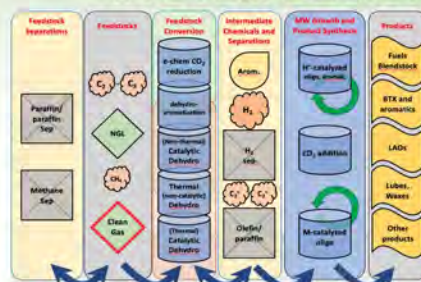
OUTCOMES

- Adsorption energies suggest weak Anderson POM-target adsorbate interaction, as the target adsorbates easily desorbs from the active site.
- Binding energy calculations reveal highly endothermic adsorption.
- Moreover, for CO adsorption, CO prefers to bind with OH to form COOH.
- Keggin Polyoxometalates exhibit promising interactions with target adsorbates.
- The interaction with the adsorbate is highly exothermic.

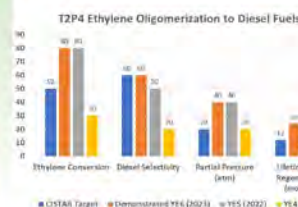
IP & INNOVATION



SYSTEM DESIGN & BENCHMARKS



Progress Toward CISTAR Target



IMPACT & FUTURE

- Establish the reaction pathway by determining the elementary steps between reactants and products.
- Use these models to guide material and system design